# NAVAL RESEARCH

## REVIEWS

MAY 1978



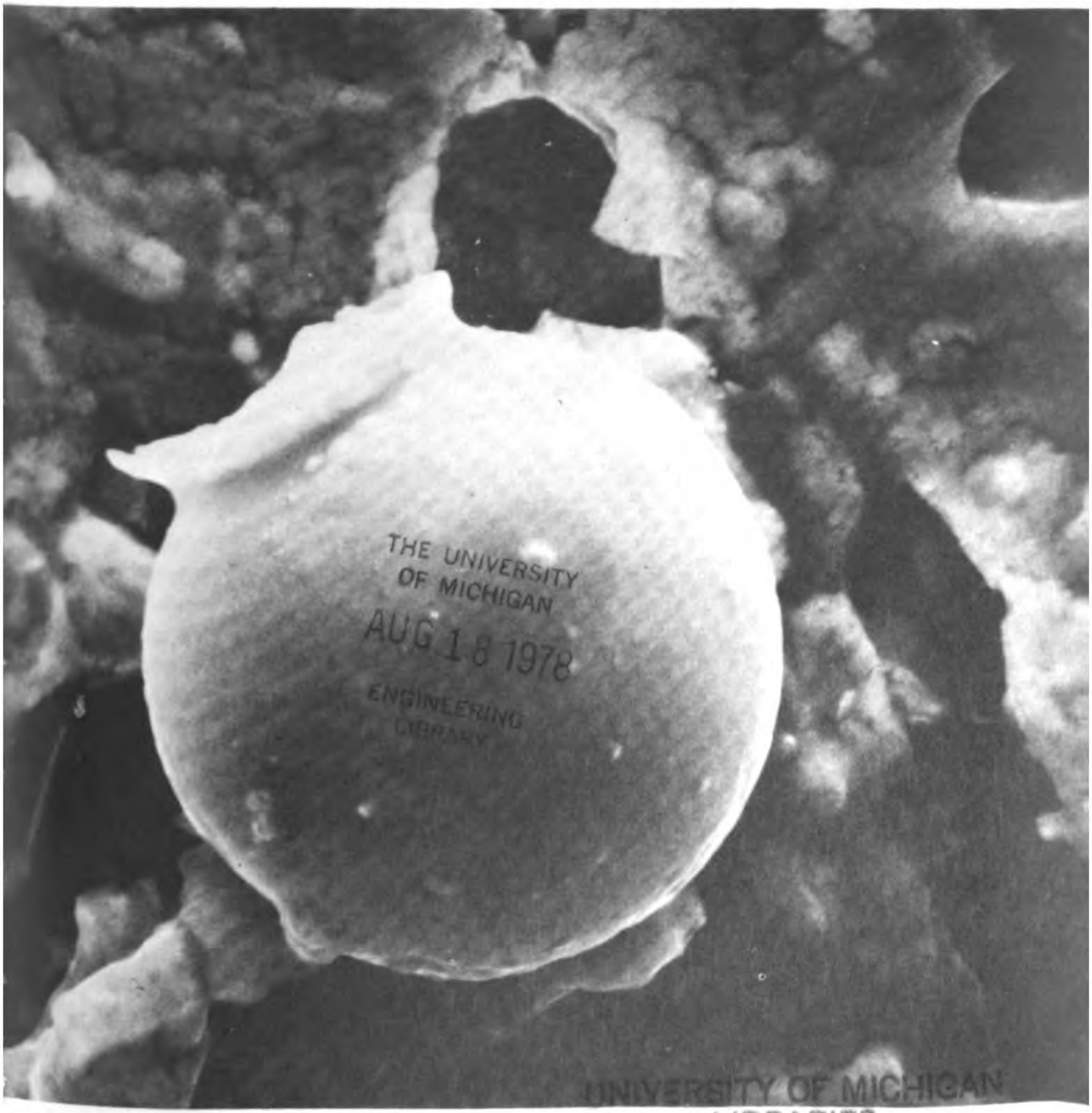

# PROFILES IN SCIENCE

*Dr. Arthur W. Guy*

Dr. Arthur W. Guy, who is a Professor in the Department of Rehabilitation Medicine and Director of the Bioelectromagnetics Research Laboratories at the University of Washington, has been an Office of Naval Research contractor for the past six years. He is well known for research on the biological effects and medical applications of nonionizing electromagnetic energy. Among his accomplishments Professor Guy is noted for pioneering new microwave dosimetry techniques utilizing synthetic tissue models and infrared thermography so that radio frequency and microwave energy absorption patterns can be quantified in the tissues of animals and man exposed to electromagnetic fields Also he developed animal exposure systems uniquely adapted to the problem of continuously providing a quantified and controlled dose rate of microwave energy to a large population of animals under normal laboratory living conditions.

Today he directs an interdisciplinary program in his laboratory partially supported by ONR covering a myriad of studies on the effect of long term low level microwave exposure on the behavior, central nervous system, blood chemistry and cells of laboratory animals.

Dr. Guy is serving on a number of National Research Council Committees charged with the evaluation of the biological hazards of nonionizing electromagnetic energy; and he is a member of the Board of Directors of the Bioelectromagnetics Society, a society for the promotion of research concerned with the interactions of electromagnetic energy and biological systems.

# Piezo- and Pyroelectricity in Poly (Vinylidene Fluoride)

**P.E. Bloomfield, R.A. Ferren, P.F. Radice, Harry Stefanou, and O.S. Sprout***
*Pennwalt Corporation*

## Introduction

Organic polymeric materials have been used extensively as electrical insulators and dielectrics. In the past few years a number of other important and useful electrical properties of polymeric materials have been investigated. Synthetic polymers are made that are photoconducting, photoluminescent, ferroelectric, polarizable, piezoelectric, and pyroelectric. This paper emphasizes the piezoelectric and pyroelectric behavior of poly(vinylidene fluoride), PVDF.

Since the discovery of piezoelectricity by the Curie brothers in 1880, continued interest has been displayed in this phenomenon because of its practical as well as theoretical significance. Piezoelectric materials transform force to an electrical response. The opposite effect also occurs; a dimensional change occurs when an electrical charge is applied to a piezoelectric material.

Pyroelectricity was also predicted in the nineteenth century by the Curies. Pyroelectric materials develop an electrical charge from a thermal change; whereas inverse pyroelectricity, or the electrocaloric effect, is of minor importance.

Practical use of the piezoelectric property of quartz was made in 1916 by Langevin, who developed an ultrasonic sending and receiving system. A piezoelectric quartz crystal was set into oscillation by an electrical signal, and the high frequency mechanical vibration was transmitted through the water to a reflecting body. A second quartz crystal received the reflected mechanical vibration (ultrasound) and, from the time lapse between sending and receiving, the distance from the source to the reflecting object could be calculated. This first major application of piezoelectricity was thus the forerunner to modern day sonar.

*The authors are part of the multidisciplinary group involved in the study of the electrical properties of polymers at the Pennwalt Technological Center, King of Prussia, PA. 19406 For many years Pennwalt has been doing research with inorganic coordination polymers for ONR.

Many applications have been commercialized for piezoelectric ceramics and more recently for piezoelectric polymer films. These applications have been broadly classified as either generator (mechanical vibration transformed into an electrical signal) or motor (electrical signal transformed into a mechanical force.)

The first piezoelectric materials discovered were naturally occurring substances such as Rochelle salt and quartz. More recently ceramics that have improved piezoelectric activity have been synthesized. The rigidity of the ceramics is great compared to polymers. This is an advantage in the efficiency of converting from one energy form to another. These brittle materials, however, are hard to make in the thin large sections that are commonplace for polymer films. Consequently, these two types of piezoelectric materials, i.e., polymeric and ceramic, are more complementary than competitive.

Naturally occurring materials such as wood and other biological substances were the first piezoelectric polymers to be investigated. Fukada[1] studied a large number of these materials. Kocharyan[2], et al., in 1967 studied a number of polar and nonpolar polymers subjected to a high voltage, high frequency field and discovered that the higher the polarity of the polymer, the higher the "induced" piezoelectric effect. They discovered that polytrifluoroethylene, plasticized polyvinyl chloride, and rigid polyvinyl chloride had the highest activity, whereas polymethyl methacrylate and polystyrene had low activity and no activity was observable with polytetrafluoroethylene.

In 1969 Kawai[3,4] discovered that PVDF could be poled to a level of activity not previously obtained with any other polymeric material. His work is especially remarkable because he recognized the importance not only of the chemical composition but also the necessity for using highly oriented specimens of a particular crystalline form.

Edelman and collaborators[5,6] at the National Bureau of Standards (NBS) were investigating the piezoelectric properties of synthetic polymeric material such as polyvinyl chloride in 1969 and have continued investigating methods to increase the activity of polymeric materials, especially PVDF. As a result of this work, Edelman's group developed a number of practical devices for applications in underwater acoustics, pressure sensors, and ignition devices.

There have been many theoretical and applied studies on the piezoelectric and pyroelectric properties of PVDF. Wada and Hayakawa[7,8] in two review articles describe and cite much of this work.

Kureha marketed capacitor film shortly after entering the PVDF market in 1967. This film, although not ideal for making piezoelectric and pyroelectric elements, led to the development by Kureha of economical piezoelectric and pyroelectric elements. The excellent research work by Kureha, Pioneer, NBS, and other companies has helped establish this technology as commercially practical. Nevertheless, this technology is still in its infancy, and there is much more to be learned about this subject.

Pennwalt was the first commercial producer and is now the only domestic manufacturer of PVDF resins. Studies on the electrical properties of PVDF have been underway since the late 1950's and significant markets have been developed for these resins. Currently the company is working with a number of investigators to develop piezo- and pyroelectric PVDF products to meet their specific needs. With partial support by the Office of Naval Research, an effort is under way at Pennwalt to discover new polymer systems exhibiting piezoelectric activity equal or superior to that of PVDF.

Although use of PVDF in the electrical field is important, other markets exist for this material, such as for exterior coatings and films and for corrosion control in the chemical process industry. Film samples of these resins have been subjected to environmental testing for twenty years with excellent results, showing the outstanding stability of these resins.

## Origin and Mechanism of Piezo- and Pyroelectricity

In a discussion of the origins and mechanism of piezoelectricity it is important to have a clear definition of the phenomenon. One that will suffice admirably is that of W. G. Cady:[9] Piezoelectricity is "electric polarizations produced by mechanical strain in crystals belonging to certain classes, the polarization being proportional to the strain and changing sign with it". It should be clear that the inverse effect is also true. That is, an electrical polarization will induce a mechanical strain in piezoelectric crystals.

The first fact to note is that only certain crystals are piezoelectric. All crystals belong to one of 32 point groups. These 32 point groups are the 32 classes of crystals known to the crystallographer. Only 20 of the 32 classes exhibit piezoelectricity and 10 of the 20 exhibit both piezo- and pyroelectricity. The common element linking these 20 groups is the absence of a center of symmetry. Hence, if a crystal is centrosymmetric, it is not piezoelectric.

The existence of a polar axis in the crystal gives rise to an inherent spontaneous polarization. The spontaneous polarization of a crystal is present before any electric field has been applied. Hence, in any treatment of piezoelectricity the spontaneous polarization should be taken into account when considering the polarizations caused by exposure to an electric field. In fact, classically, any abnormally large piezoelectric constant may owe its existence to a spontaneous polarization.

Given the elastic nature of crystals, the imposition of a stress results in a strain. A piezoelectric material has the property that a polarization is produced or an already existing polarization is changed when the material is strained. An electrical stress due to an applied electric field will also produce electrical polarization and elastic strain in a piezoelectric material. Similar to piezoelectricity, pyroelectricity is a linear reversible

effect. For example, a temperature change produces thermal contributions to the strain and the polarization. See Table 1 for formal relations between these electrical, mechanical, and thermal quantities.

Table 1
Piezoelectric Quantities and Coefficients

| | | |
|---|---|---|
| 1. $\epsilon/\epsilon_0 = \mathrm{K} = 1 + \chi$ | 3. $k = ge$ | 5. $D = dX + \epsilon^X E + p^X \Delta T$ |
| 2. $d = s^E e = \epsilon^X g$ | 4. $D = \epsilon_0 E + P$ | 6. $S = s^E X + dE + \alpha^E \Delta T$ |

1. Relative permittivity K in terms of dielectric susceptibility $\chi$.

2. The piezoelectric strain constant $d$ and the pizoelectric stress constants $g$ and $e$ are related by means of the elastic compliance $s^E$ (reciprocal of Young's modulus) and dielectric constnat $\epsilon^X$.*

3. The electromechanical coupling constant $k$ in terms of $g$ and $e$.**

4. The electric displacement $D$ in terms of the electric field $E$ and polarization $P$.

5. $D$ in terms of electric field $E$, stress $X$, temperature change $\Delta T$, and pyroelectric coefficient $p^X$.

6. Strain $S$ in terms of $X$, $E$, $\Delta T$, and thermal expansion coefficient $\alpha^E$.

*When the temperature is held constant the *d, e, and g* constants can be described as follows: From (6) $d$ is the amount of strain needed per unit change of electric field to maintain constant stress and can be measured in meters per volt. Alternatively from (5) $d$ is the amount of charge per unit area evoked per unit of stress change under constant field conditions as measured in units of Coulombs per Newton. Furthermore, $e$ is the stress induced by an applied $E$-field under constant strain or the surface charge developed for given applied strain under constant $E$-field. Finally $g$ gives the electric field developed across the material resulting from an applied stress under open circuit conditions.

**The ratio of the converted mechanical or electrical energy output to the electrical or mechanical energy input is given by $k^2$.

The piezo- and/or pyroelectricity exhibited by many polymers have been explained by essentially three phenomena. They are:

(1) The intrinsic piezo- and pyroelectricity due to the symmetry of the lattice.

(2) The piezo- and pyroelectric activity due to the strain and temperature dependence of the spontaneous polarization which may be

inherent in the polymer crystals. (Alignment of the crystals' polar axes in an electric field introduces a metastable macroscopic polarization in the polymer film giving rise to the piezo- and pyroelectricity.)

(3) Piezo- and pyroelectricity due to the introduction of an asymmetric charge distribution and or asymmetric mechanical and electrical properties of the polymer influencing an embedded charge distribution.

Mechanism (1) suffices to explain piezoelectric activity that is not abnormal in magnitude while mechanisms (2) and (3) have been used to explain unusually large piezo- and pyroelectric activity such as that observed in PVDF. At present, the results of Pennwalt's investigations[12] are in agreement with those of investigators favoring mechanism (2) (polarization due to dipole alignment) as the predominant mechanism.

In order to discuss why mechanisms (2) and (3) are feasible for PVDF, a brief description of the polymer's structure is needed. PVDF is a semicrystalline polymer, $(CH_2 - CF_2)_n$, with a melting point that falls in the range 150-180°C, depending on the method of synthesis. The glass transition temperature is at approximately −40°C and therefore thermal motion in the amorphous regions would readily randomize any cooperative phenomenon. Thus when discussing piezo- and pyroelectricity one examines the crystal phase more closely. Crystalline PVDF exists in three phases designated $\alpha$, $\beta$, and $\gamma$. The $\alpha$-phase predominates when the polymer is cooled from the melt, whereas the $\gamma$-phase results under more exotic conditions. The $\beta$-phase is of primary interest because it has been shown that piezo- and pyroelectricity are correlated with $\beta$ content.[10] The $\beta$-phase forms when $\alpha$ crystals are stretched or PVDF is cast from certain solutions. X-ray diffraction analysis has shown that the unit cell of the $\beta$ crystal is orthorhombic, belonging to the $C_{2v}$ (mm2) crystal class[11]. This implies that the $\beta$ crystals are both piezo- and pyroelectrically active.[3,4,9] In addition, examination of the chain structure reveals that the carbon-fluorine dipoles can interact in a cooperative and additive manner in the chain and, as well, in the crystal. Figure 1 depicts the planar zig-zag chain conformation in the $\beta$ crystal form of PVDF. The structure of the $\alpha$-phase is a twisted non-polar configuration and therefore the $\alpha$ phase is not expected to show the kind of spontaneous polarization that the crystals of the $\beta$-phase have been postulated to have. The piezoelectric activity of PVDF containing predominantly $\beta$-phase crystals is roughly an order of magnitude larger than that containing predominantly $\alpha$-phase crystals. Several investigators have reported evidence that the dipoles of the $\beta$ crystals align with the electric field during poling.[13,14,15]

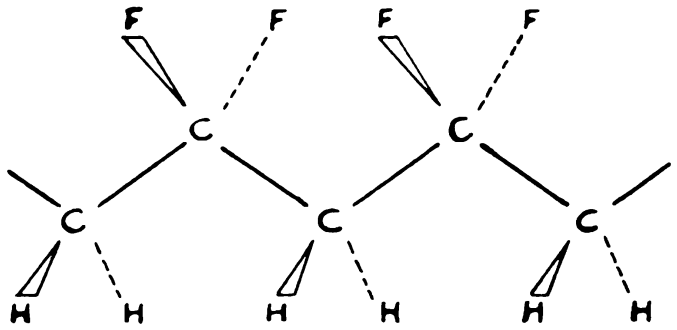


*Figure 1 — The planar zig-zag conformation of PVDF in the β-phase.*

Other polymers besides PVDF have the planar zig-zag chain conformation, and, if the crystal structure is right, they should exhibit piezoelectricity. Table 2 lists some polymers with highest activity and their corresponding d constats. Copolymers rich in vinylidene fluoride are piezoelectrically active but are not included in the Table.

Table 2
A Comparison of the Piezoelectric Activity
of Some Polar Polymers with
Planar Zig-Zag Chain Conformations

| | $d_{31}\left(\frac{\text{Picocoulombs}}{\text{Newton}}\right)$ |
|---|---|
| β-Poly(vinylidene fluoride) | 26.0-50 |
| Poly(vinyl fluoride) | 0.99-1.32 |
| Poly(vinyl chloride) | 0.33-0.49 |
| Nylon 11 | 0.49 |

Clearly, the planar zig-zag structure with additive dipole arrangement is not necessary for piezoelectric activity, but it is necessary for invoking mechanism (2) as the origin of the activity. We have noted that mechanism (3) involves a distribution of charges. The origins of these charges are under intense study, the rationale being that if the origin of a charge layer is proved then the mechanism is proved. There are several theories of charge injection from electrodes; for example, thermal emission as in the Richardson-Schottky effect or electric-field assisted tunnelling from the electrodes as in Fowler-Nordheim field emission. Also, charge carriers can arise from internal field emission of impurities, the Poole-Frenkel effect. Each of these mechanisms requires that the charge be trapped in a manner that renders the asymmetric distribution thermally stable. Workers have postulated that the β crystals in PVDF are trapping sites. In any case the study of the

dependence of each of these charge introduction mechanisms on field, temperature, electrode metal, polymer thickness, and time should elucidate which, if any, is operating. Experiments have been performed with "blocking films" that would prevent charge injection and different electrode metals to enhance Schottky emmission.[10,16,17] However, the results of such experiments are inconclusive. Whether the dipole orientation or charge injection or both mechanisms are responsible for piezo- and pyroelectricity in PVDF remains to be resolved.

## Properties of Piezoelectric and Pyroelectric PVDF

PVDF films are partly crystalline and partly amorphous, the crystalline portion ranging between 35 and 40%. When PVDF films are initially extruded, the non-piezoelectric, non-polar $\alpha$-crystal phase predominates. As mentioned above, drawing (stretching) or rolling the film at elevated temperatures causes partial transformation to the piezoelectric polar $\beta$-phase. After the film is poled (and stabilized by heating[18] and/or pressing[19] under shorted condition), essentially permanent polarization results.

As in non-centrosymmetric crystals and ceramics, hysteresis loops are swept out when measurements of polarization versus applied E-field are made on piezoelectric PVDF. Thus this piezoelectric polymer can be considered ferroelectric.

The electric permittivity of oriented $\beta$-phase film is somewhat higher than $\alpha$-phase film.[20] In the range 100 Hz to 100 kHz the permittivities are approximately frequency independent. See Table 3. Strong anisotropy is observed in the elastic coefficients and consequently in the piezoelectric coefficients of highly drawn uniaxially oriented films. They are stiffened in the draw direction, termed direction 1, while the elastic modulus is lowered in the width direction 2, and the thickness direction 3. Because the thin polymer films from which piezoelectric devices are fabricated have strong directional properties, it is important to note that the piezoelectric stress and strain constants are subscripted matrices relating vectors of polarization or E field to tensors of mechanical stress or strain. For example, $d_{31}$ is a polarization in the 3-direction caused by a stress in the 1 direction. Typical room temperature values of the piezoelectric d-constants and the electromechanical coupling constants, k, for PVDF are given in Table 4.

Table 3
Room Temperature Relative Permittivity, K

| | 0.1 Hz | $10^2$-$10^5$ Hz | 10 MHz |
|---|---|---|---|
| $\alpha$-phase | 14 | 10 | 5 |
| $\beta$-phase | 20 | 12 | 5 |

Table 4
Typical Room Temperature Values of Piezoelectric Constants, $d$(pC/N) and $k$ (%)

| | | |
|---|---|---|
| $d_{33} = -30^*$ | $d_{31} = 24$ | $d_{32} = 4$ |
| $k_{33} = 19$ | $k_{31} = 15$ | $k_{32} = 3$ |

*Extension in the thickness direction produces opposite-signed charge to that for extension in the plane of the film.

The polymer melting point is a pseudo-Curie temperature. This was made particularly evident in studies on a copolymer prepared by Pennwalt (73% vinylidene fluoride, 27% tetrafluoroethylene with melting point 125°-130°C). In experiments carried out at NBS (Gaithersburg) partially supported by the Office of Naval Research and Naval Undersea Systems (NUS, San Diego) in which polarization was induced at the melting temperature and the film was cooled in the applied field, the resulting room temperature piezoactivity was significant (d = 8 pC/N) and persisted undegraded up to the melting point. This copolymer has the property that all the crystalites occur in $\beta$-phase, so that prestretching is unnecessary to effect an $\alpha$ to $\beta$ transformation. However, at Pennwalt and at the Watertown Arsenal[21] it has been found that stretching the already pure $\beta$-phase copolymer film before poling enhances its piezoactivity by factors of two to four. These findings indicate that stretching enhances the piezoactivity of the pure PVDF film not only by effecting an $\alpha$ to $\beta$ transformation but also through other orientation effects.

In Table 5 are listed various physical properties of PVDF piezoelectric film.[20,22-25] Transducers made from PVDF film are thin and flexible and have low density and excellent stability to shock. They can be prepared in arbitrary shapes. Their flexibility allows them to be wrapped around objects having sharp curvatures. PVDF is mechanically tough and its piezoelectricity is highly stable. Its compliance is ten times greater than the compliance of ceramics, and its g-constant is very high. Piezoelectric PVDF polymer film can be made into wideband electroacoustic transducers with high coefficients of voltage generation per unit stress. The flat frequency response over a wide range (d.c. to many MHz) is a consequence of the polymer's softness, which eliminates the self-ringing found in brittle materials. A comparison of the physical constants of PVDF and other piezoelectric materials is presented in Table 6. Note that the acoustic impedance (Z) in Table 5 refers to the 3-direction. However the velocity of sound (c) exhibits a strong anisotropy; so that the acoustic impedance ($Z = \rho c$) in Table 6 pertains to the 1-direction for which the sound velocity is 1.4 km/sec.

## Table 5
## Physical Properties of PVDF Piezoelectric Film
## (Typical Values)

| | | | |
|---|---|---|---|
| Melting Point | 165°-180°C | Acoustic Impedance | $4 \times 10^6$ kg/s·m$^2$ |
| Flammability | self-extinguishing | Volume Resistivity | $10^{13}$ Ω·m |
| Thermal Conductivity | 0.13 W/m-°K | Dielectric Strength | 150-200 MV/m |
| Specific Heat | 2.5 MJ/m$^3$ °K | Relative Permittivity (60 Hz-100 kHz) | 12 |
| Specific Gravity | 1.8 | | |
| Tensile Strength | 200 MN/m$^2$ | Piezoelectric Strain Constant, $d$ | 25 pC/N |
| Young's Modulus | 1500 MN/m$^2$ | Piezoelectric Stress Constant, $g$ | 0.23 V·m/N |
| Sound Velocity, $c$ | 2.2 km/s | | |
| Thermal Expansion Coefficient, $\alpha$ | $1.4 \times 10^{-4}$/°K | Pyroelectric Coefficient, $p$ | 40 $\mu$C/m$^2$·°K |
| | | Detectivity (at 4 Hz) | $10^{11}$m·Hz$^{1/2}$/W |

## Table 6
## Comparison of Physical Constants between Piezoelectric Crystals and PVDF

| | Density $\rho$ ($10^3$ kg/m$^3$) | Dielectric Constant $\epsilon/\epsilon_o$ | Piezoelectric Strain Constant* $d$ ($10^{-12}$ m/V) | Voltage Output Coefficient* $g$ ($10^{-3}$ V·m/N) | Coupling Coefficient* $k$ (%) | Acoustic Impedance* $Z$ ($10^6$ kg/m$^2$·sec) |
|---|---|---|---|---|---|---|
| Quartz O°X | 2.65 | 4.5 | 2. | 50 | 10 | 14.3 |
| Rochelle Salt 45°X | 1.77 | 350 | 275 | 90 | 73 | 5.6 |
| $BaTiO_3$ ceramic | 5.7 | 1350 | 78 | 5.2 | 21 | 30 |
| PZT ceramic | 7.5 | 1700 | 110 | 10 | 30 | 30 |
| PVDF | 1.76 | 12 | 20 | 190 | 14 | 2.5 |

*Length Extensional Mode

### Poling of Polymer Films

Polymeric films are normally made pyro- and piezoelectric by the operation of "poling". This procedure generally consists in the application of a direct current electrical field to a film inserted between surface electrodes while the assembly is heated and finally cooled to ambient temperature. Also known as polarization, the process results in the structural and electrical responses described previously. The poled film may exhibit a transient external electrical field as well as transient internal polarization. Both can be dissipated without loss of a persistent internal polarization. Deliberate expulsion of the transient internal polarization constitutes the step of stabilization. Permanent internal po-

larization occurs to an especially signi .ant degree in poled PVDF and its copolymers.

The initial properties of the PVDF film have a critical effect on the poling operation and the characteristics of the poled film. Films for poling have been prepared from solution or dispersion casting, or by blowing or extruding a melt of the resins, extrusion being most frequent. Unoriented films have been poled, but orientation of the polymer chains in the plane of the film is necessary to attain enhanced piezoelectric activity. Orientation is accomplished by stretching uniaxially along one face dimension, usually in the direction of machine travel, or biaxially, in both machine and transverse directions. Film elongations of about three to seven times the original dimension have been employed, preferably in the upper range. Film thickness depends on the caliper of the base stock and the stretching conditions and ordinarily ranges from about five to 50 micrometers (25.4 $\mu$ m - 0.001" = 1 mil), although much thicker sections such as plaques or slabs have been of interest.

Film for poling is usually coated on one or both sides with aluminum, chromium, gold, nickel, silver, or another metal to provide an intimate electrical contact with the film during poling as well as in subsequent use. The coatings, also referred to as electrodes, are best applied by vacuum deposition; but conductive paints, tapes and foils are sometimes used. However, unmetallized film can be poled and subsequently metallized when necessary.

The significant parameters for poling are electrical field strength, temperature, and time, discussed individually below. Under some combinations of these conditions, the dielectric material may demonstrate a propensity to fail by short-circuit and rupture, known as breakdown or burn-through. The quality, thickness, and area of the film to be poled may also contribute to this tendency.

The strength of the applied electrical field is almost invariably expressed in relation to the thickness of the poled film, most commonly as kilovolts per centimeter. Field strengths of 1,000 kV/cm (100 MV/m) and above are frequently used, but excellent piezoelectric activity can be attained at lower field strengths, particularly if the properties of the film are favorable. Piezoelectric activity increases with increasing field strength; however, it begins to level off at higher field strengths. There appears to be a threshold value at about 150 kV/cm (15 MV/m) below which only minimal activity may result. Any current during poling is small.

Poling temperatures up to 140°C have been used for PVDF, the melting point of the polymer composition to be poled imposing limitations. Piezoelectric activity increases directly with poling temperature although this progression becomes limited at higher temperatures. It has been reported that decreasing the poling temperature from 100°C to 20°C greatly reduces the growth rate of the pyroelectric coefficient of

6-$\mu$ m PVDF films, but not the coefficient ultimately attainable by prolonged poling (about one week).[26] Some observers, however, have indicated that permanent polarization of 50-$\mu$ m PVDF film may require poling temperatures above about 60°C and that the permanent polarization saturates above about 110°C.[27] Poling at excessive temperatures may in fact diminish piezoelectric activity as a consequence of film relaxation and loss of orientation effects.

Piezoelectric activity also increases with poling time to a limited extent. Under favorable conditions, poling times much beyond 30 to 45 minutes may be of little benefit. Reactions to the electrical field appear to be practically instantaneous; several observers report responses from poling for one second or less. It has been reported that poling for a few seconds at field strengths of 200-400 MV/m has resulted in high activity.[28,29] The effects of time are obscured in part because of the different poling schedules adopted by various workers. It now appears that final cooling under the applied field can be greatly shortened or perhaps eliminated.

Laboratory procedures for poling can be scaled-up to a modest degree by increasing the size of the film sheets and conducting a number of individual polings concurrently. In a more convenient and larger volume method, a stack of an even number of layers of metallized film is wound around a core to form a roll. The layers are arranged in such a manner that the film surfaces that contact each other are identically charged during poling, thus preventing breakdown.[30] A continuous poling method has also been described.[31] Here, a roll of film is continuously fed through an oven or around a heating drum. In either case, electricl contact is established by charged rollers. A series of transverse unmetallized strips occur on at least that face of the film which will contact the charged rollers. The distance between the unmetallized strips is such that contact always exists with one of the charged rollers.

Polarization methods other than the aforesaid classical procedure have been reported. In one such method, film was successfully polarized in a corona discharge at room temperature or below for a period of a minute or less.[32]

## Application of PVDF Poled Elements

### Piezoelectric Transducers

Piezoelectric transducers are made from poled and stabilized PVDF films. The thickness range is generally 5 to 50 $\mu$m, and typical areas are 1-100 $cm.^2$ The devices are either freely mounted or applied with an adhesive to a solid or flexible frame or backplate. In contrast to conventional transducer materials, PVDF has very wide-band characteristics and has been employed as a transducer at frequencies from d.c. up

to GHz. It is possible to employ these film transducers in either the length extension mode or the thickness extension mode. Transducers can be fabricated in a large number of different shapes and sizes by very simple techniques.

## Audio

Electro-acoustic transducers such as microphones, stereophonic headphones, tweeters, and phonograph cartridges have been developed with PVDF films. An extremely simple microphone may be constructed by using a small disc of polarized film. The only mounting requirements are electrical shielding and the absence of resonance within the casing. Such a microphone is lightweight, has good sensitivity, and operates from zero to above 20 kHz. This compares favorably in performance with the electret or condenser microphone and does not have the drawback of the moisture sensitivity of the electret microphone or the d.c. voltage requirement of the condenser microphone. The piezoelectric-element microphone develops elongation and contraction motion by the sound pressure applied to the film, resulting in the generation of voltage between the electrodes on the film. Second generation noise cancelling microphones have recently been developed using two PVDF film diaphragms.[33]

PVDF piezoelectric films are made commercially into speakers and headphones by Pioneer Electronics Corporation. The operating principle is such that when voltage is applied to the metal electrodes deposited on both sides of the piezoelectric film used as the diaphragm, elongation and contraction develop in the stretching direction of the film. When an a.c. field is applied to the film along the Z-axis, the film vibrates in a transverse direction (X-axis) as shown in Figure 2a. When the film is curved as shown in Figure 2b, the transverse vibration is converted into a pulsating movement. As a result the PVDF film

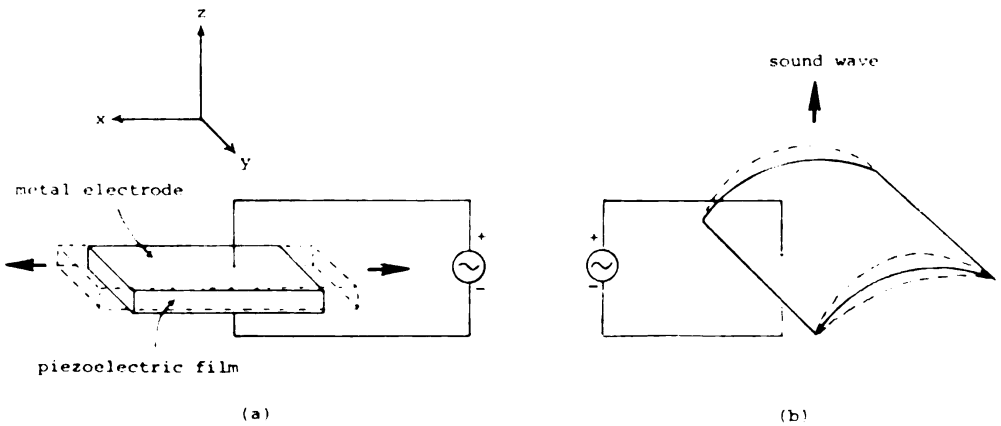


*Figure 2 — Diagrams showing longitudinal operating mode of piezoelectric film and how transverse vibration is converted into a pulsating movement.*

efficiently radiates sound. Stereophonic headphones have been commercialized in which each diaphragm has a thickness of 8 $\mu$ m and an area of 40 cm.$^2$ A 100 dB sound pressure level (SPL) is generated with only a 3V signal input. The frequency response is flat between 20 Hz and 20 kHz, and the distortion is below 1 per cent at 110 dB SPL.[34] A high fidelity speaker system has been produced having a cylindrically shaped PVDF film tweeter that is practically omni-directional over the horizontal plane. In one speaker system, the PVDF film thickness is 30 $\mu$ m, the cylindrical radius is 60 mm and its height is 90 mm.[34] The PVDF piezoelectric films are used for wideband application and high-fidelity reproduction.

A phonocartridge has been developed by an American company, Micro-Acoustics. The phonocartridge, the QDC-1 is interchangeable with the electro-kinetic cartridge. The cartridge utilizes the bending of the PVDF piezoelectric element to obtain an output voltage.

### Underwater Transducers

Underwater transducers have been constructed and are promising in sonar applications because PVDF has an acoustic impedance quite close to that of water. Several prototypes have been designed and successfully tested by NBS (Gaithersburg), NUS, and Naval Underwater Systems Center, New London, Conn. Such transducers can function in the thickness extension mode as well as the longitudinal extension mode. There are also ongoing programs to develop piezoelectric polymer hydrophones for towed, fixed, and hull-mounted arrays. PVDF arrays have also been developed for underwater acoustical imaging.

### Pressure Switches

PVDF film, when used as a finger pressure sensor or "switch" unit, produces a voltage when activated. Two types of switches are possible, either a bimorph type in which the PVDF is attached to a spring sheet that is deformed when the switch is operated or a more simple type that is activated by direct action of finger pressure across the thickness of the film. The output can be used to operate a liquid crystal display device or high impedance logic circuitry.[35] An array of such switches is used in novel keyboards.

### Pyroelectric Transducers

The advantages of PVDF as pyroelectric transducers are the moderately high Curie temperature, toughness of the thin films, moisture insensitivity, chemical inertness, and low cost. Consequently, PVDF is used although it is slightly less sensitive than conventional materials.

To fabricate a pyroelectric detector from a piece of polarized PVDF, it is necessary to allow for heat absorption. When the thermal energy is received as infrared radiation, absorption can be achieved in various ways:

a) Absorptions can occur by the front electrode or by an applied absorbing black layer.

b) A thin transparent front electrode allows absorption to occur within the plastic film.

Other modes of heat absorption can occur when the pyroelectric film is coupled with various heat transfer media.

PVDF detectors can be used as radiometers. A variety of instruments has been developed at NBS and elsewhere. Among these instruments is the Electrically Calibrated Pyroelectric Radiometer.[36] Other pyroelectric applications include temperature monitors, fire alarms, and copying equipment.

## Other Piezoelectric Applications of PVDF Polymer Film

a) Sonobuoys
b) Ultrasound transducers for non-destructive testing of structures
c) Transducers for underground pressure changes
d) Accelerometers
e) Intrusion devices
f) Traffic sensors
g) Ultrasound vibration monitors
h) Pressure monitors for printing presses
i) Electrical energy supply (e.g., batteryless flash system)
j) Delay lines in computers and communications systems
k) Hearing aids

## References


[1.] E. Fukada, *Ultrasonics,* **229** (Oct. 1968).
[2.] N.M. Kocharyan, Kh. B. Pachadzhyan, and Zh. Tivriktsyan, *Dokl. Akad. Nauk. Ann. SSR,* **44** (3), 111 (1967).
[3.] H. Kawai, *Japan J. Appl. Phys.,* **8,** 975 (1969).
[4.] H. Kawai, *Oyo Butsuri,* **38** (12), 1133 (1969).
[5.] S. Edelman, S.C. Roth, and L.R. Grisham, *Shock and Vibration Bull.,* **39,** No. 2, 1 (1969).
[6.] S. Edelman, L.R. Grisham, S.C. Roth, and J. Cohen, *J. Acoust. Soc. Am.,* **48,** 1040 (1970).
[7.] Y. Wada and R. Hayakawa, *Japan J. Appl. Phys.,* **15,** 2041 (1976).

[8.] R. Hayakawa and Y. Wada, *Fortschr. Hochpolym. -Forsch.*, **11,** 1 (1973).
[9.] W.G. Cady, "Piezoelectricity", McGraw Hill Book Co., New York, London, 1946.
[10.] N. Murayama, T. Oikawa, T. Katto, and K. Nakamura, *J. Polymer Sci., Polymer Phys. Ed.*, **13,** 1033 (1975).
[11.] Ye. Gal'perin, L. V. Strogulin, and M.P. Mlenik, *Vysokomol. Soedin.*, **7,** 933 (1965).
[12.] Manuscript in preparation.
[13.] M. Latour, *Polymer,* **18,** 278 (1977).
[14.] R.G. Kepler and R.A. Anderson (In Press).
[15.] J.P. Luongo, *J. Polymer Sci., A-2,* **10,** 1119 (1972).
[16.] K. Takahashi, N. Lee, R.E. Salomon, and M.M. Labes, *J. Appl. Phys.*, **48,** 4694 (1977).
[17.] D.K. Das Gupta and R.S. Brockley, Conference on Electrical Insulation and Dielectric Phenomena, 1977.
[18.] Y. Igarashi and H. Kakutani, U.S. Patent 3660736 (1972).
[19.] P.F. Radice, U.S. Patent 4055878 (1977).
[20.] C.M. van der Burgt, G.A. van Maanen, and J.W. Vegt, "Ultrasonics International 1977", Brighton, U.K. (28-30 June 1977).
[21.] R.J. Shuford, A.F. Wilde, J.J. Ricca, and G.R. Thomas, Proc. of the 1976 Army Sci. Conf. 3, 217 (ADA 039090).
[22.] J. Hoshi, *Mod. Plast.*, **48 110 (1971).**
[23.] J.E. Dohany, A.A. Dukert, and S.S. Preston III, *Ency. Polym. Sci. and Tech.*, **14,** 600 (1971)
[24.] R.L. Peterson, G.W. Day, P.M. Gruzensky, and R.J. Phelan, Jr., *J. Appl. Phys.*, **45,** 3296 (1974).
[25.] R.J. Shuford, A.F. Wilde, J.J. Ricca, and G.R. Thomas, *Polym. Eng. and Sci.*, **16,** 25 (1976).
[26.] W.R. Blevin, *Appl. Phys. Lett.*, **31,** 6 (1977).
[27.] G. Pfister, M. Abkowitz, and R.G. Crystal, *J. Appl. Phys.*, **44,** 2064 (1973).
[28.] K. Takahashi, R.E. Salomon, and M.M. Labes, *Bull. Amer. Phys. Soc.* **23,** No. 3, HH3 (March, 1978).
[29.] G.T. Davis and J.E. McKinney, *A.C.S. Org. Coatings and Plastics Chem. Preprints* **38,** No. 1, p. 271 (March, 1978).
[30.] S. Yoshikama, T. Sasaki, and T. Ichii, U.S. Patent 3943614 (1976).
[31.] T. Sasaki, T. Ichii, and S. Terasaki, U.S. Patent 3985914 (1976).
[32.] P.D. Southgate, *Appl. Phys. Lett.*, **28,** 250 (1976).
[33.] K. Iwama, et al., JEE, **115,** 35 (1976).
[34.] H. Naono, et al., Audio Engineering Society Preprint No. 1271 (0-1) (1977).
[35.] H.R. Gallentree and R.M. Quilliam, *Marconi Review,* Fourth Quarter, 1976).
[36.] G.W. Day, et al., *Ferroelectrics,* **10,** 99 (1976).

# Spheroids Produced by Cavitation Erosion

**Alagu P. Thiruvengadam***
*Daedalean Associates, Incorporated*

There is a growing need for the ability to predict, control and prevent unscheduled downtime of industrial equipment through a better understanding of the mechanisms of formation of wear particles. The size, shape and distribution of particles are closely related to various mechanisms of wear and erosion. Recent observations of spherical particles in bearing surfaces and lubricating oils (1) have generated much interest in understanding the mechanisms producing spherical particles. It has been suggested by some investigators (2,3) that cavitation in bearings may be an important mechanism in the formation of spherical particles.

In order to explore the possibility that cavitation erosion does indeed generate spherical particles, controlled experiments were conducted using the ASTM (American Society for Testing and Materials) standard vibratory apparatus. Conclusive evidence that spherical particles were produced by conventional cavitation erosion was reported in reference (3) as early as 1973. More detailed investigations were conducted by producing cavitation erosion on annealed SAE 52100 bearing steel and 1100-F aluminum in SAE 10W nondetergent lubricating oil, in methanol and in distilled water. Specialized techniques for isolating and mounting the wear particles were developed. The particles were examined by means of a specially built bichromatic light microscope, an electron probe microanalyzer and a scanning electron microscope (SEM). The range of sizes observed in this study varied from 0.5 $\mu$ to 30 $\mu$. Perfectly smooth spherical particles were observed in both oil and distilled water. A greater number of spheriods were observed in the aluminum-oil combination than in any other combination.

These interesting observations were further continued under the sponsorship of the Office of Naval Research. Scanning electron microscope observations on the surfaces of the test specimens revealed numerous craters and overflowing lips. In light of these results, the various mechanisms proposed by previous investigators for explaining

*Dr. Thiruvengadam is Chairman of Daedalean Associates, Inc., Springlake Research Center, 15110 Frederick Road, Woodbine, Maryland 21797. His contributions to the understanding of the phenomena of cavitation and erosion are well known.

the formation of spherical particles were re-examined. All of the available evidence indicated that the high strain rate indentation resulting from cavitation bubble collapse led to plastic flowing of the metal into the surrounding fluid where surface tension produced spherical particles. The mechanism is similar to a rain drop splashing into a pond and producing a tiny spherical spray. Further experiments were conducted utilizing a cavitating high speed jet. Spherical particles as large as 150 $\mu$ in diameter were produced in these experiments. In addition, needle shaped particles supporting the splash mechanism were also discovered during these studies. The long-range objectives of these studies are: 1) to identify the size and shape of the eroded particles; 2) to analyze and understand the mechanisms that produce these particles; and 3) to develop methods through which the erosion phenomena may be identified and prevented.

## Experimental Techniques and Procedures

The experimental facilities used for these studies include the ASTM standard vibratory cavitation erosion apparatus and the Daedalean Associates, Inc. cavitating jet apparatus. The vibratory apparatus used in these experiments consist of a commercially available piezoelectric transducer, velocity transformer, power supply, oscilloscope and voltmeter. A photograph of this apparatus is shown in Figure 1. Since an

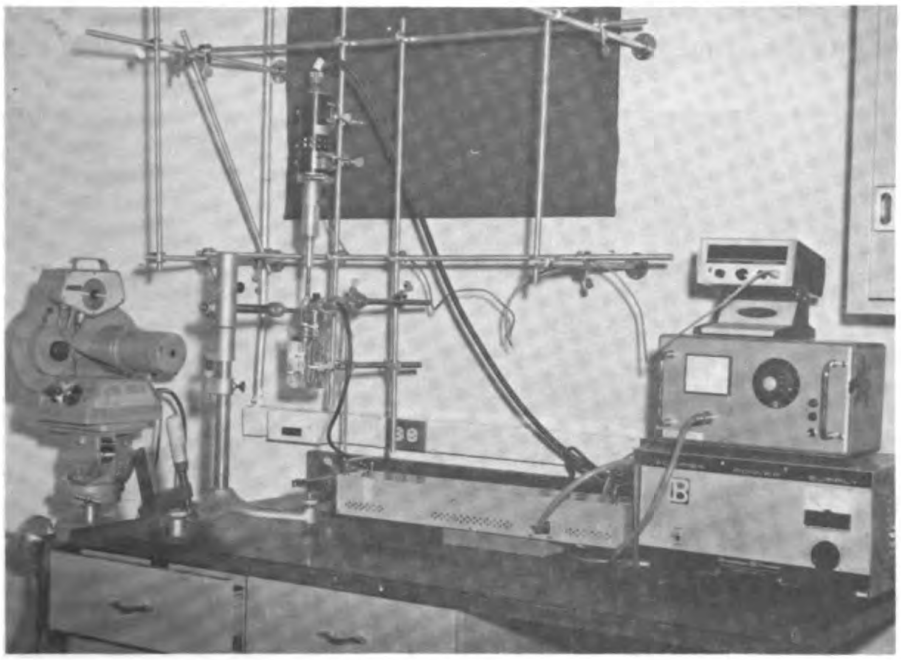

*Figure 1 — ASTM standard vibratory apparatus produces cavitation erosion in a beaker containing the test liquids including water, methanol and lubricating oils. The test specimen vibrates at 20 kHz frequency at an amplitude of one thousandth of an inch. Spherical particles on the order of 10 microns in diameter have been observed in this apparatus.*

appreciable amount of heat is generated from the acoustic energy radiating from the test specimen, a constant temperature bath is used to cool the test liquid. Tests with distilled water and methanol were conducted in glass beakers. When testing the test specimens in oil, however, the oil would erupt and splash out of the open beakers. Therefore, narrow necked glass containers fitted with Styrofoam washers were used during the tests. The eroded particles were generally allowed to settle on the bottom of the beaker. Sometimes it was necessary to use a magnet to force these particles to the bottom of the beaker when the fall velocity of the particles was low due to the smaller size of the particles and the higher viscosity of the test liquid. The particles were collected and mounted on glass slides for examination under a light microscope as well as under a scanning electron microscope. In order to fix the particles onto the slide, a diluted soap solution was sprayed on the slide.

In addition, we also use a high velocity jet erosion apparatus to produce these spherical particles. In this apparatus, a submerged jet cavitates under water and erodes materials in relatively short periods of time. The eroded debris is collected from the flow system and analyzed using the techniques developed for the vibratory apparatus.

## Spheroids Produced By Cavitation Erosion

In general, the eroded particles were quite irregular in shape and showed a large degree of plastic deformation prior to failure. Scanning electron micrograph of a typical sample of particles shown in Figure 2 represents the range of sizes and shapes observed in the erosion debris.

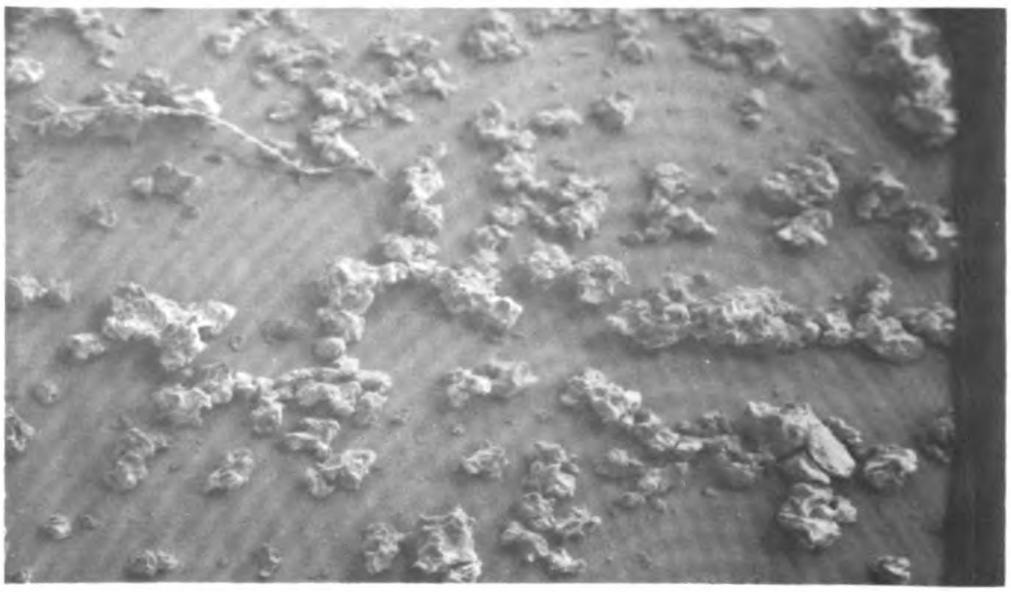

*Figure 2 — Scanning electron micrograph of a typical sample of particles shows the range of sizes and shapes observed in the erosion debris. The size distribution varied from one micron to 30 microns. Most of the particles were irregular in shape and showed severe plastic deformation, fatigue striations and concave and convex surfaces.*

The size distribution varied from 0.5$\mu$ to 30$\mu$. Most of the particles were irregular in shape and showed severe plastic deformation, fatigue striations and concave and convex surfaces. This particular sample was obtained in the vibratory erosion apparatus using 1100-0 aluminum as the test material in distilled water. However, this sample is typical of other materials tested in liquids other than water such as methanol and lubricating oil.

Closer examination of individual particles showed clearly the extent of plastic deformation undergone by these particles before fracture and separation from the test surface. Figure 3 shows a micrograph of a single erosion particle at a magnification of 3000X. The sharp edges and striations on the bottom right of the picture are indications of brittle fracture as a result of repeated bubble collapse and fatigue failure. Moreover, a large number of particles showed hemispherical concave dents on their surfaces as shown in Figure 4. Some of these particles were also seen twisted as seen on the lower left-hand corner of Figure 4. We observed another set of particles containing shallow and deep blow holes on their surface appearing as though some hot gases escaped from the interior of the particle while it was cooling rapidly (Figure 5).

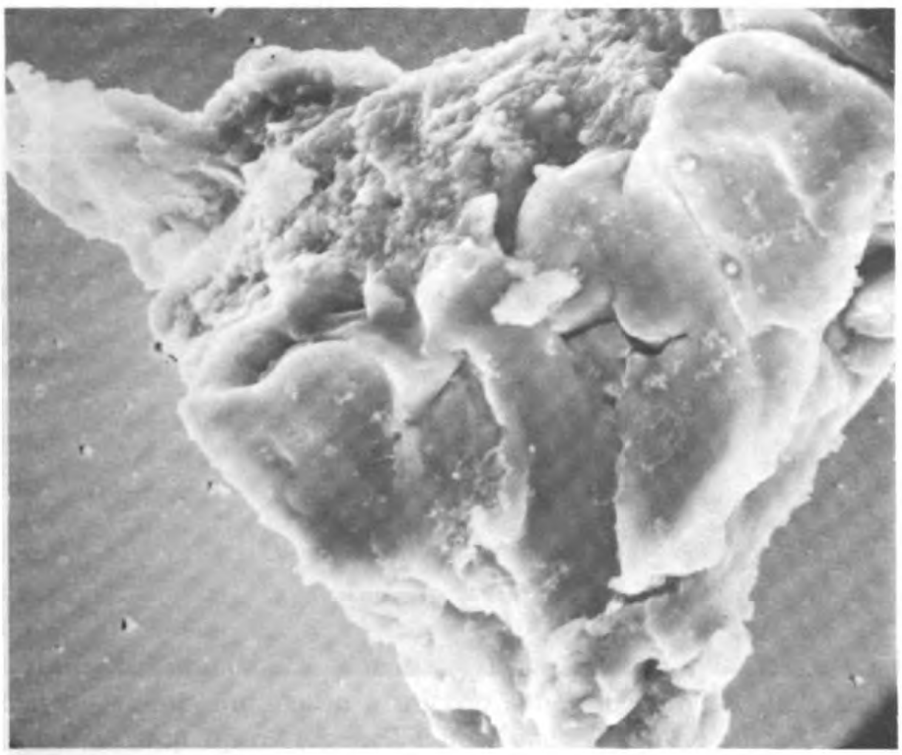

*Figure 3 — This SEM photomicrograph of a single erosion particle at a magnification of 3000X shows the details of plastic deformation of the aluminum material on upper left of the picture. The sharp edges and striations on the bottom left indicate brittle fracture as a result of repeated bubble collapse and resultant fatigue failure.*

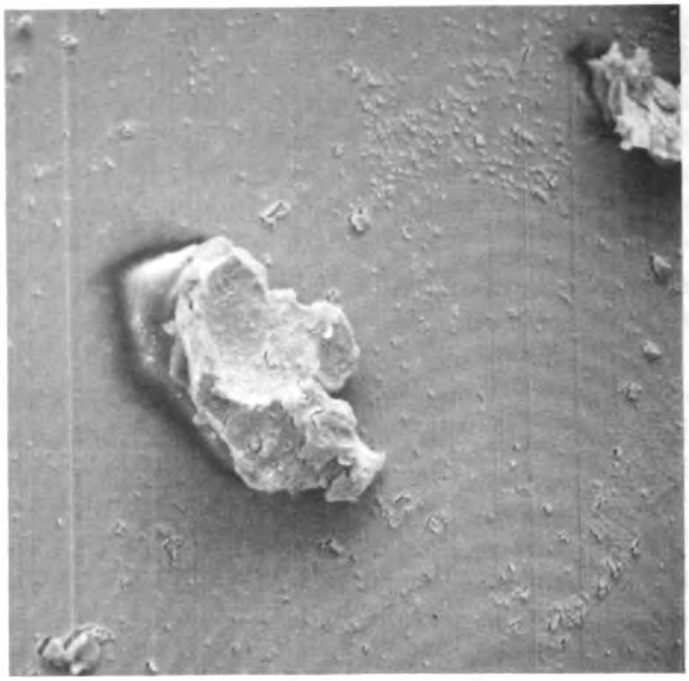

(a)

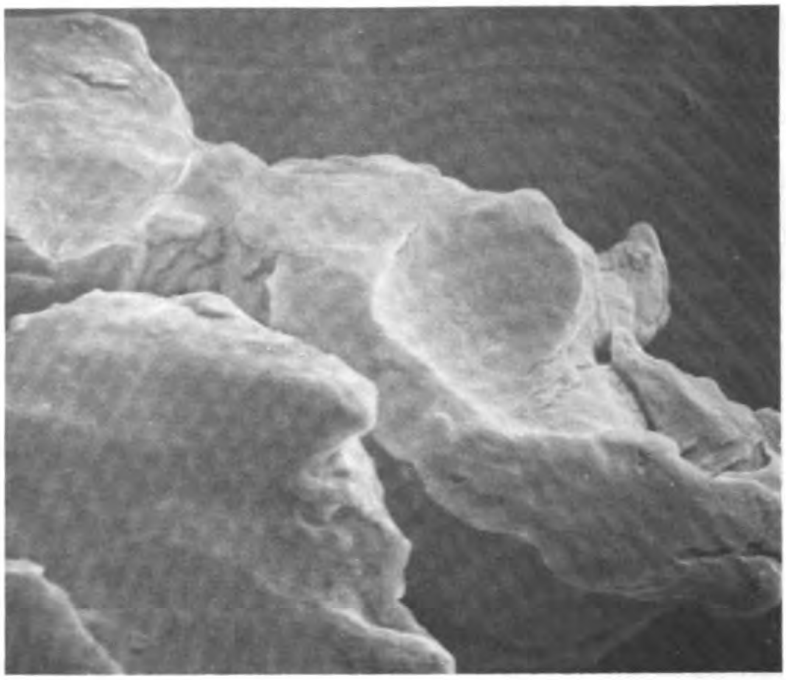

(b)

*Figure 4 — Hemispherical concave dents were observed on the eroded particles shown in this SEM micrograph shown in Figure 4a. Some of these particles were also seen twisted as indicated on the lower left-hand corner of Figure 4b.*

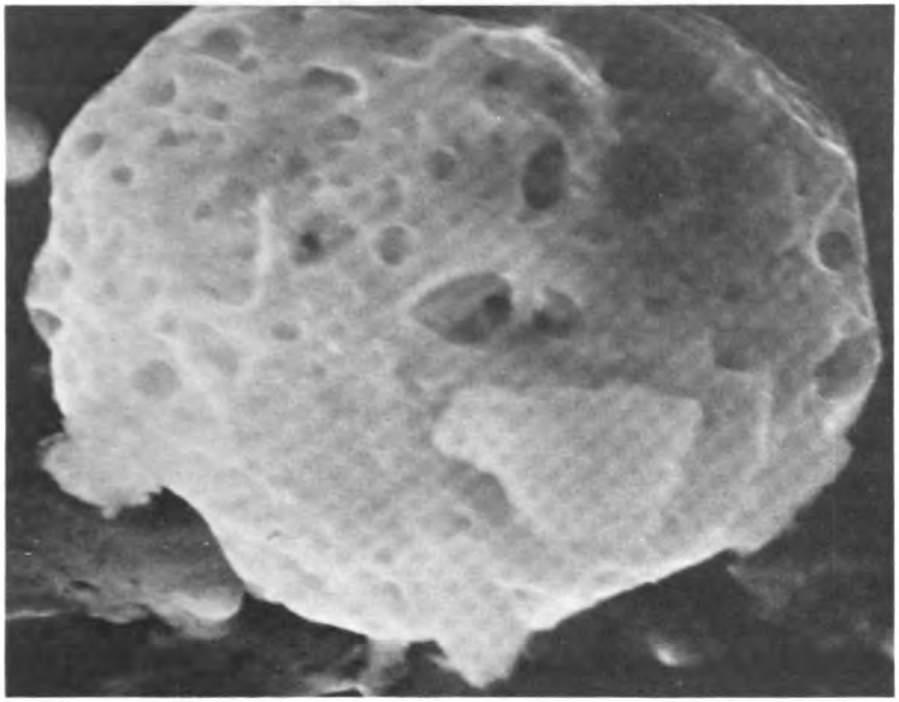

*Figure 5 — This particle shown at a magnification of 5000X exhibited shallow and deep blow holes on its surface. A closer examination of several of these particles seemed to indicate as though some hot gases escaped from the interior of the particle while it was cooling rapidly.*

Most interesting among these particles is the occurrence of spherical particles as shown in Figure 6. The sizes of these spheres ranged from 0.5$\mu$ to 30$\mu$ in diameter among the particles obtained in the vibratory apparatus. However, their sizes and frequency of occurrence increased significantly (up to 150 microns in some cases) when the jet erosion apparatus was used to produce these spheroids. The peel-like layer on this spheriod is the gold coating used for the purpose of the SEM photographic technique employed in this case. These spheroids stand out clearly among other particles. Detecting these spherical particles among the erosion debris was not a major problem. Figure 7 shows another spheroid which illustrates this point well. In this case, the gold film was much thinner, and the surface smoothness as well as the relative size is demonstrated clearly in these pictures. Most of these spheres exhibited a characteristically smooth surface. Their surface appeared to be mirror-like, highly polished and smooth when viewed through a bichromatic light microscope with a high numerical aperture. Figure 8 illustrates this observation on a 5 micron spheroid with the help of the image of the sharp tip of a pencil point focused on the surface of this spheroid. To obtain this image, we introduced a sharp pencil tip in the line of sight and focused the image of the tip on the surface of the sphere. The light reflected area in Figure 8 is about one or two microns in diameter on the surface of a 5 micron sphere.

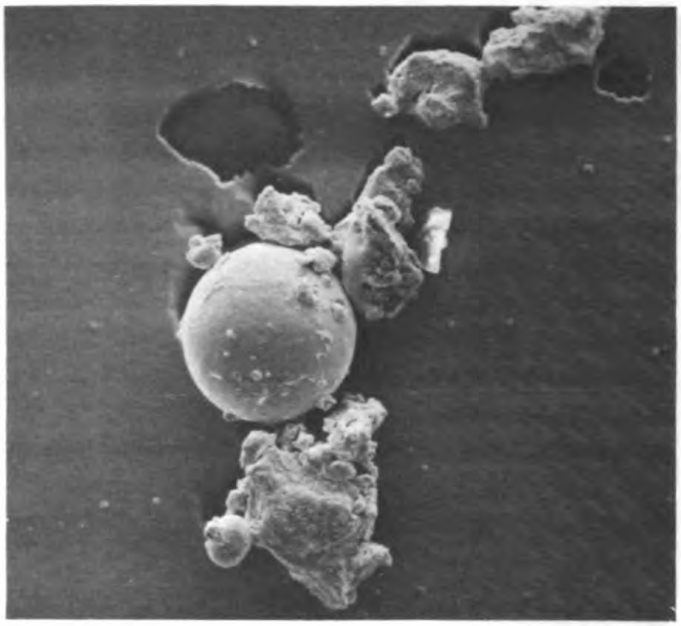

(a)

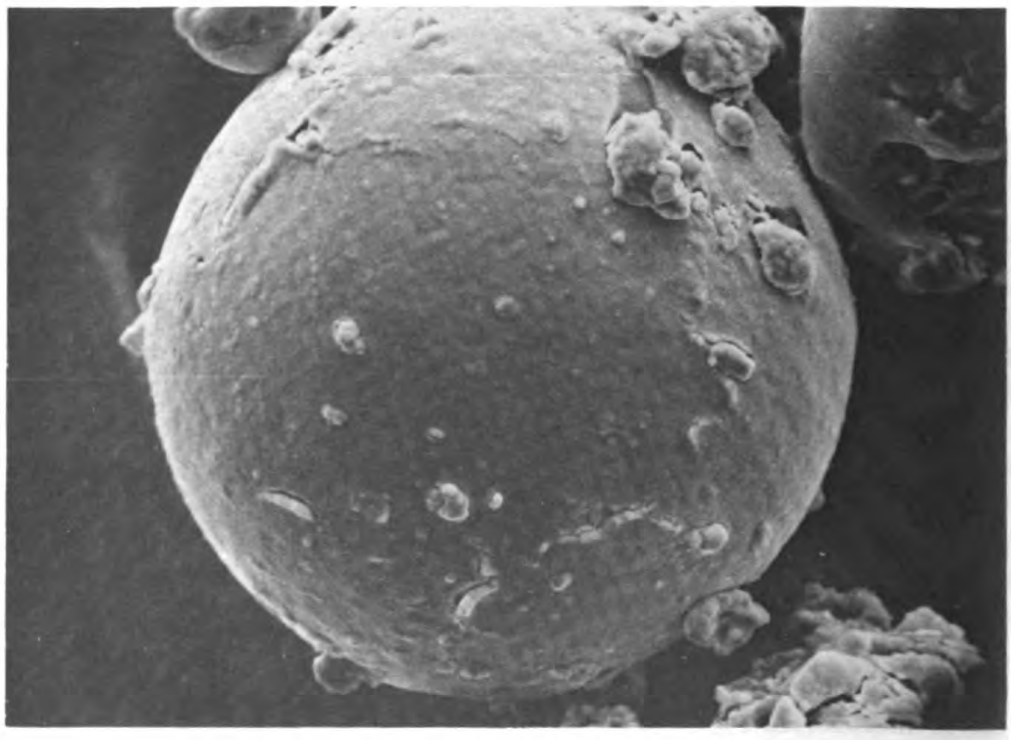

(b)

*Figure 6 — Most interesting among them is the occurrence of spherical particles as shown in this SEM micrograph. These spheres ranged from one micron to 30 microns in diameter among the particles obtained in the vibratory apparatus. However, their size increased considerably (up to 150 microns in some cases) when the jet erosion apparatus was employed. The peel-like layer on this spheroid is the gold coating used for the purpose of SEM photographic technique. Note the relative size of the spheroid in relation to the other irregular particles in Figure 6a.*

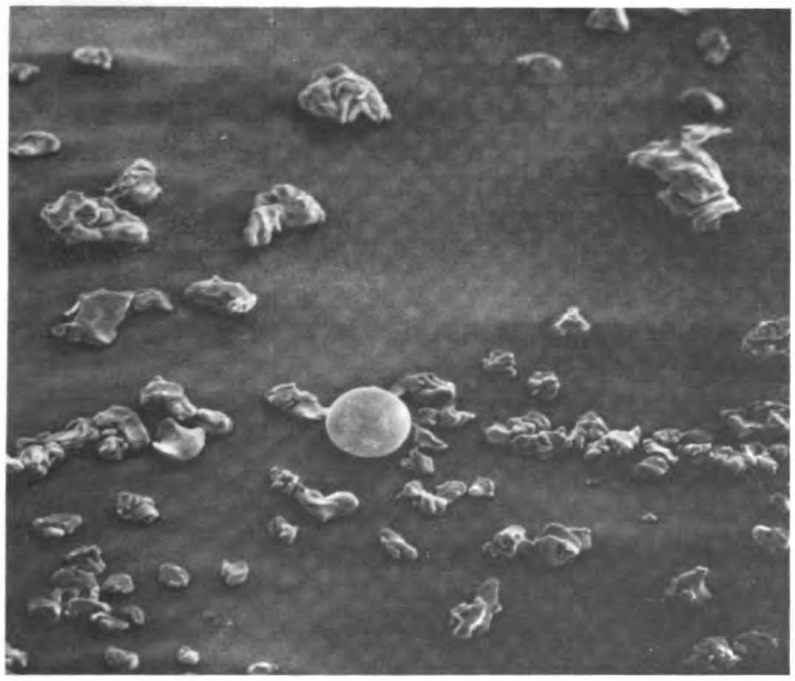

(a)

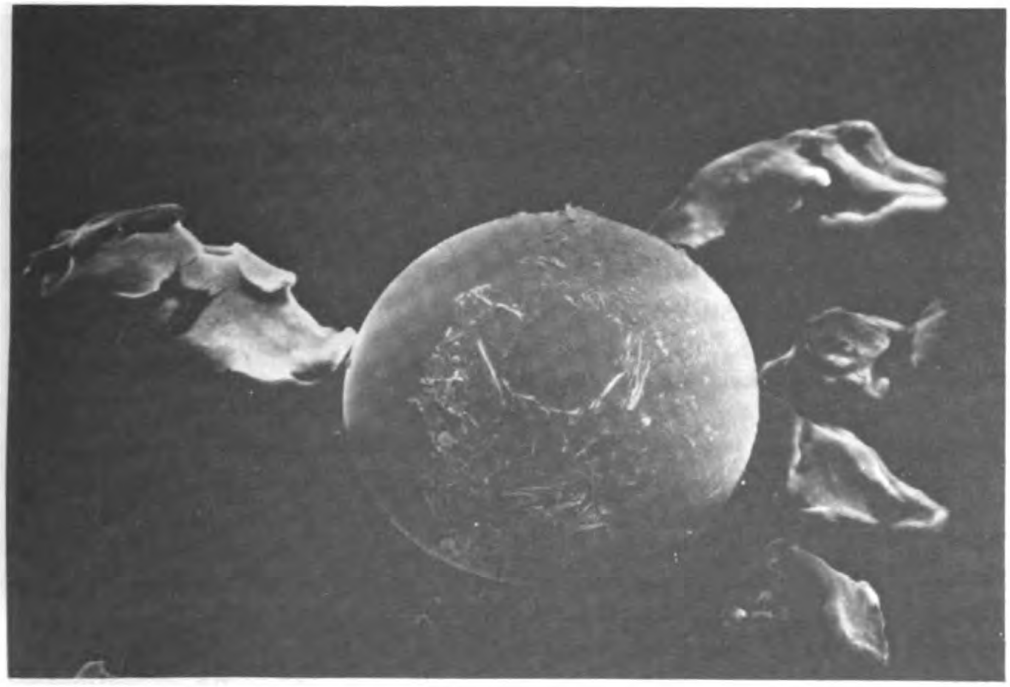

(b)

*Figure 7 — Another spheroid is shown in this SEM picture among the erosion debris. The gold coating on this particle is relatively thin. The interesting observation in this picture is the very smooth surface of these particles. Moreover, they usually stand out distinctly among other particles so that their identification has never been a problem.*

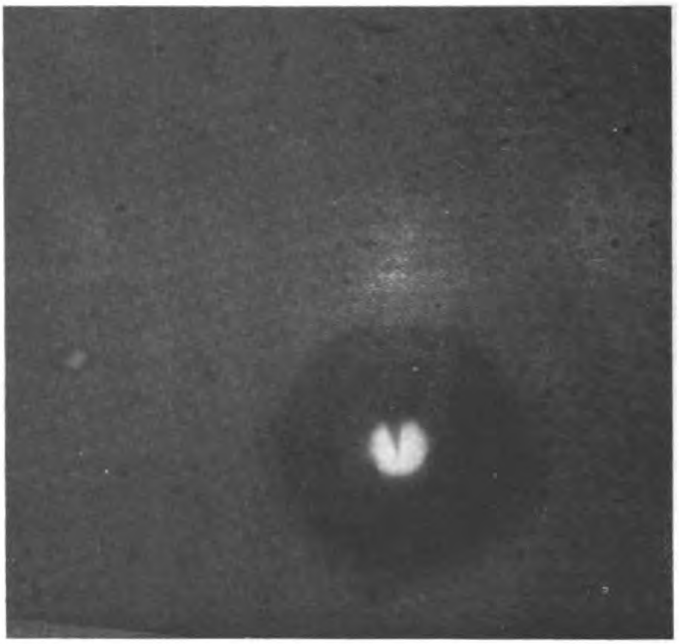

*Figure 8 — This photomicrography of a 5 micron spheroid was obtained with the help of bichromatic light microscope with a high numerical aperture. The reflected light from the surface of the spheroid indicated the extreme smoothness of the surface. They appeared like highly polished mirror like surfaces. To illustrate this fact, we introduced a sharp pencil tip in the line of sight and focused the image of the tip on the surface of the sphere as shown in this photograph. One could see a perfect image of the pencil tip on the top surface of the 5 micron sphere in an area covering about one or two microns in diameter.*

Some of the spheres underwent very rapid corrosion process as shown in Figure 9. When spherical particles of 52100 bearing steel were produced in distilled water using the vibratory apparatus, the particles looked like glowing orange balls in the bichromatic microscope. The surface was again very smooth except for a very thin coating of what seemed like oxide layer. It is interesting to note the perfect shape of the spheroid and the ring of light shining on its surface. This particular spheroid was about 3 microns in diameter. Similar size spheroids were produced in SAE 10W nondetergent lubricating oil using 52100 steel and the spheroids were highly polished with bright metallic lustre. There was no orange colored film observed on their surfaces. In order to verify if these spheroids were made of the test material or of some other organic matter, such as oil-water globules (as some investigators speculated), we examined them in a scanning electron microprobe analyzer. Figure 10a shows the X-ray scan for steel whereas Figure 10b shows the same for aluminum in the spheroids obtained with aluminum as the test material. These X-ray micrographs confirmed that these par-

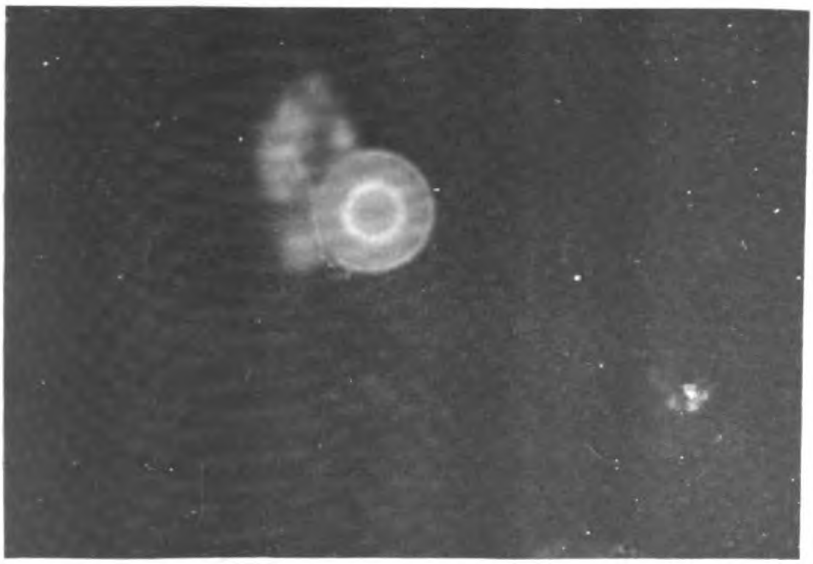

*Figure 9 — When spherical particles of 52100 bearing steel were produced in distilled water using the vibratory apparatus, the particles looked like glowing orange balls in the bichromatic microscope. The surface was again very smooth except for a very thin coating of what seemed like oxide layer. Notice the perfect shape of the spheroid and the ring of light shining on its surface. This particular spheroid was about 3 microns in diameter. Such a uniform and smooth coating of oxide layer on a three micron sphere was a very interesting observation.*

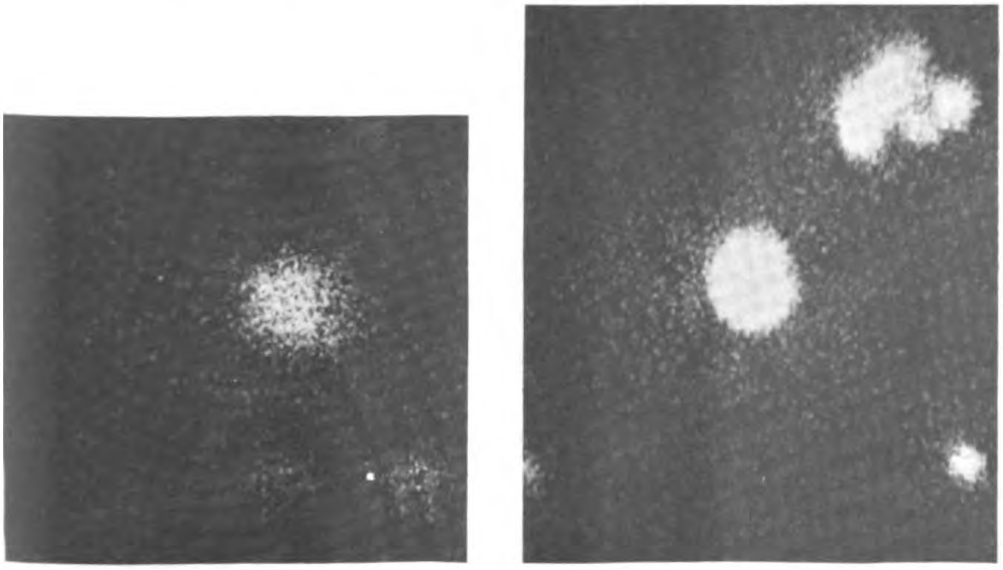

**(a)** **(b)**

*Figure 10 — In order to verify if these spheroids were made of the test material or of some organic matter such as oil-water globules, we examined them in a scanning electron microprobe analyzer. Figure 10a shows the X-ray scan for steel in the spheroids obtained with 52100 bearning steel whereas Figure 10b shows the same for aluminum in the spheroids obtained with aluminum as the test material. It was confirmed conclusively that these spheres were made of the parent test material.*

ticles were indeed made of the same materials as the parent material being eroded.

As early as 1970, Scott and Mills (1) proposed a mechanism by which these spheroids may be produced in the case of rolling contact wear failure phenomenon. They found evidence which showed that the spherical shaped debris could be formed from tongues of metal removed by a cavitation erosion process due to the application and release of extreme pressure in the lubricant. More recently, Loy and McCullum (4) observed a relationship between sphere formation, the generation of white-etching areas and the failure of bearing balls by pitting. They found sphere development in the white-etching areas beneath wear tracks on bearing balls. They suggested that the spherical particles on pitted surfaces might be generated by a subsurface mechanism connected with fatigue crack development. According to their hypothesis, the material located between the ends of two approximately parallel cracks in different planes became highly deformed and the cracks propagated around this knot of work hardened material. All of the above observations and hypotheses were related to the formation of spherical particles at pitted, abraded and fretted metal surfaces. However, our attempts to use these mechanisms to explain the formation of spheroids produced by cavitation erosion were not too successful.

Detailed and systematic observations of the eroded surfaces of different materials were made and the salient results are reproduced in the next few figures. When a smooth surface of soft lead plate was exposed to cavitation bubbles, the bubble collapses producing crater like indentations almost instantaneously (Figure 11). One could easily see

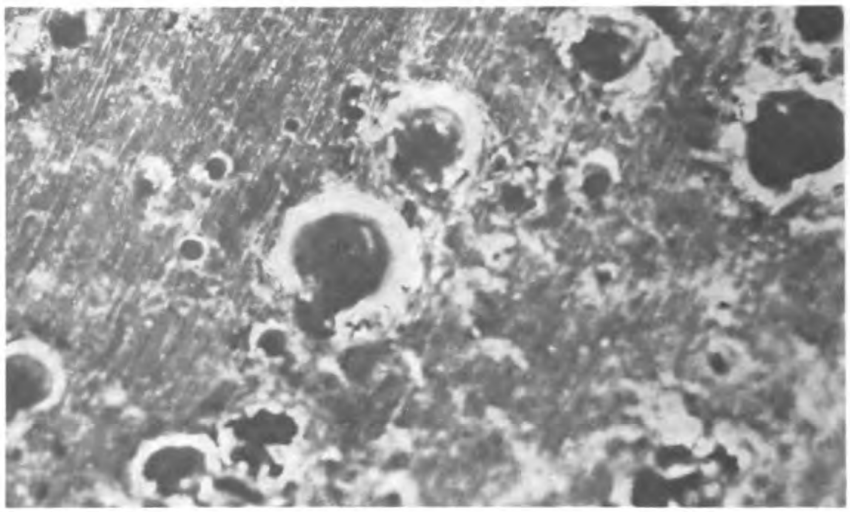

*Figure 11 — An understanding of the mechanism of these spheroids was sought through careful observations of the eroded surfaces. When a smooth surface of a soft lead plate was exposed to cavitation bubbles, the bubble collapses producing crater like indentations almost instantaneously. One could easily observe the overflowing side lips around the rim of the craters. These craters ranged from 100 microns to 1000 microns in diameter.*

the overflowing side lips around the rim of the craters. These craters ranged from 100 microns to 1000 microns in diameter. When the material was exposed to a higher intensity of cavitation bubble collapse, multiple craters overlapping each other as shown in Figure 12 were observed on aluminum. These craters varied form 60 to 800 microns in diameter. Inner surfaces of these craters showed severe pitting and plastic deformation. Further close-up views of these craters showed many smaller craters inside the larger craters (Figure 13a). Further magnification of these smaller craters revealed severe plastic flow and overflowing lips as shown in Figure 13b. One could also see a partially formed spheroid sitting on top of the rim of one of these craters as shown in Figure 13c. These observations threw some additional light on how cavitation bubbles produced material deformation and erosion in addition to a possible theory of how the spheroids might be formed.

As early as 1917, Rayleigh (5) showed that high pressure waves were produced during the collapse of a spherical bubble. Recent attention has been focused toward an understanding of the formation of liquid jets caused by nonspherical collapse (6). When such a shock wave or a microjet impinges on the material with enough intensity, the

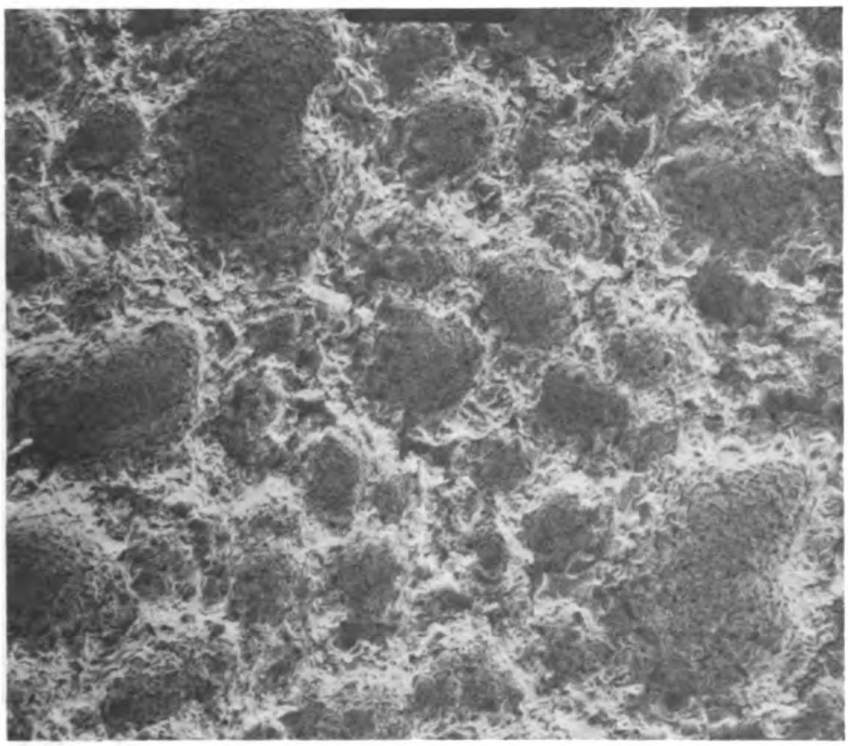

*Figure 12 — When the material was exposed to a higher intensity of cavitation bubble collapse, multiple craters overlapping each other as shown in this figure were observed on aluminum. These craters varied from 60 to 800 microns in diameter. Inner surfaces of these craters showed severe pitting and plastic deformation.*

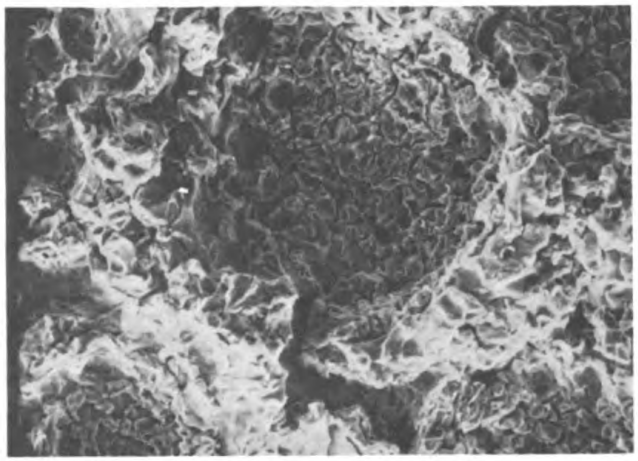

(a)

(b)

(c)

*Figure 13 — A close-up view of one of these craters showed many smaller craters inside the larger craters as shown in this SEM micrograph (Figure 13a). Further magnification of these smaller craters showed severe plastic flow and overflowing lips as shown in Figure 13b. One could also see a partially formed spheroid sitting on top of the rim of one of these craters (Figure 13c). Such observations led to a possible theory of how the spheroids might be formed. Moreover, these micrographs threw some additional light on how cavitation bubbles produced material deformation and erosion.*

material is likely to flow plastically due to the extremely high rates of deformation and associated high temperatures. According to this hypothesis, the material splashes out during the process of cratering (Figure 14) into the surrounding test liquid and the spherical droplets of the splashing material solidify almost immediately in the test liquid.

An artist's concept of how the cratering process might occur is shown in Figure 14. This is based on the photographic evidence obtained by Dr. Edgerton several years ago. He dropped a milk droplet on a stationary surface of milk and observed the splash mechanism. During this process, he found that there was a sheet of rim around the crater. From this sheet emanated several needle-like stems as shown in Figure 14. Small spherical particles broke off from the stem before the particles fell back into the surface again. We collected several particles

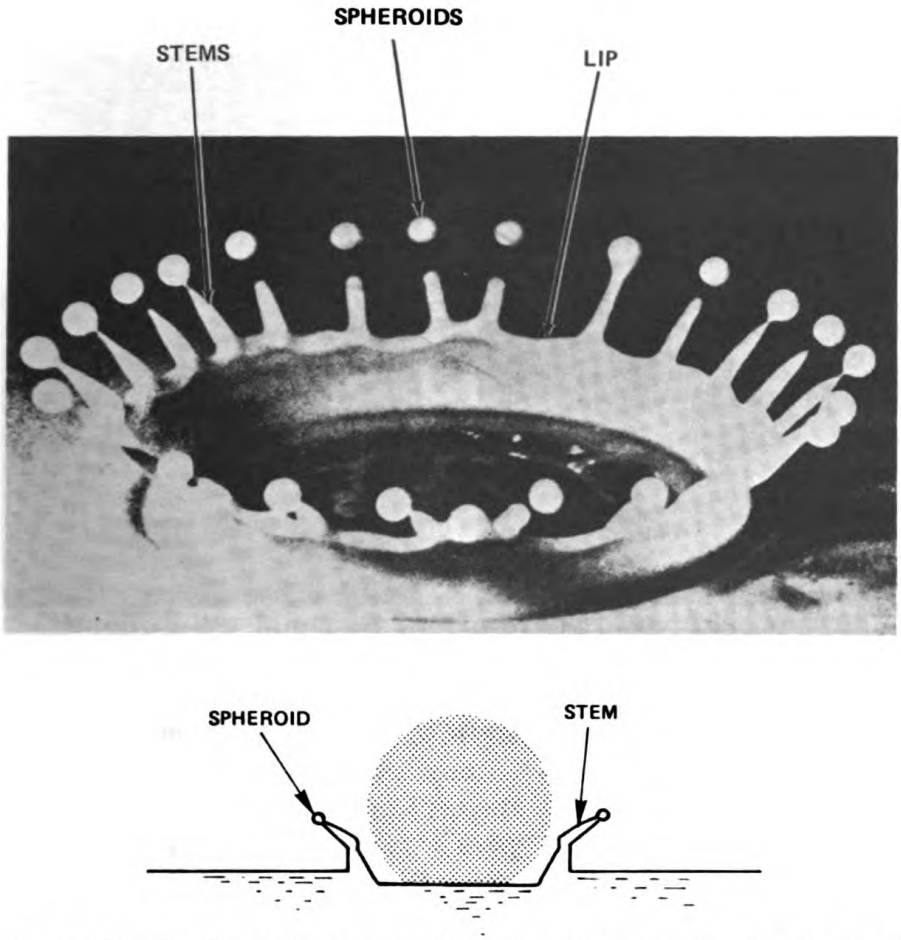


*Figure 14 — This figure shows an artist's concept of how the material might splash during the high rate of deformation and cratering. It is very similar to the milk drop impact on a stationary surface of the milk; such phenomena were photographed by Dr. Edgerton several years ago. During the process of cratering and associated splashing a continuous surface along the rim of the crater is formed. Needle-like protrusions extend from the rim. Spherical particles break away from these needle shaped stems.*

with different shapes that would fit into the splashing mechanism. For example, the cover picture shows a partially formed sphere that was found among the aluminum debris from the vibratory apparatus. One could clearly see the break away portion of the stem attached to the spherical particle. The erosion debris from the jet erosion apparatus contained clusters of spheroids and needle-like stems. A typical stem is shown in Figure 15; their diameters ranged from 50 to 150 microns. The diameters of the spheres also varied in the same range. The diameter of the spheroid in relation to the stem is shown in Figure 15b. The largest spheriod observed so far is about 150 microns in diameter. Further work is under progress in developing a quantitative theory that would predict the size of these spheroids in various materials under controlled conditions.

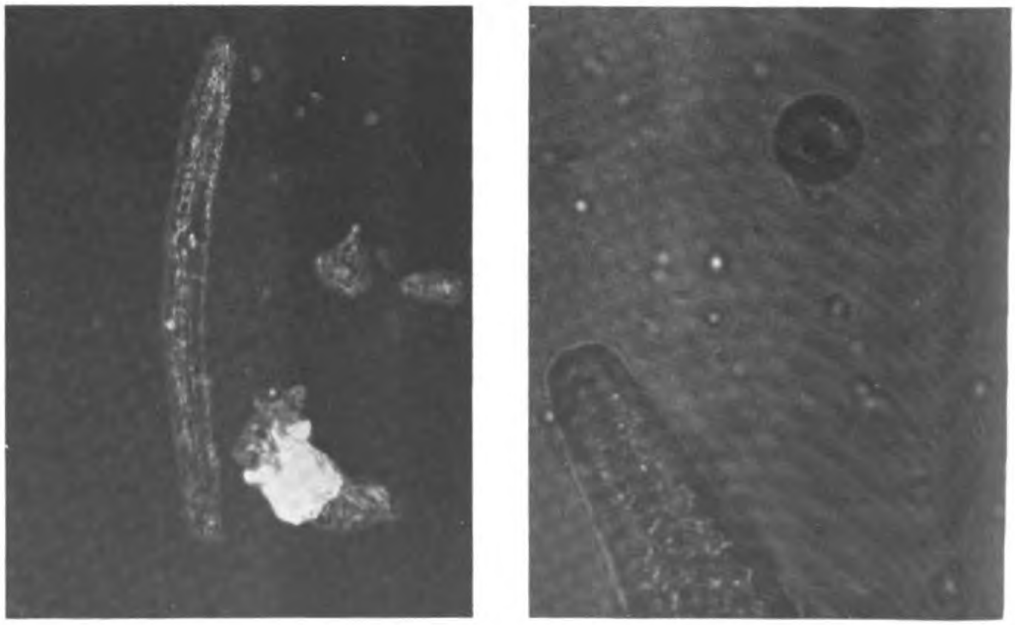

(a) (b)

*Figure 15 — Evidence of the stem-like particles were found in large numbers among the erosion debris of the jet impact apparatus. The diameter of the spheroids in relation to the size of the tip of the stem is shown in Figure 15b.*

## Concluding Remarks

Investigations completed so far indicate that cavitation erosion can be an important mechanism producing spherical particles in the wear debris. In the vibratory cavitation erosion experiments, more spheroids were observed among the particles from the erosion of aluminum in oil. The size of the spheroids ranged from 0.5 to 30 $\mu$. The average of these spheroids was in the range of 10 to 15$\mu$. Much larger spheroids

up to a maximum diameter of 150$\mu$ were observed in the jet cavitation erosion apparatus. Moreover, a greater number of spheroids were observed in clusters along with long cylindrical and needle shaped particles. The diameter of the cylindrical particles were of the same size as the diameter of the spheroids. Scanning electron microscopic studies indicated ample evidence for the splash mechanism of formation of these particles. According to this mechanism, it is hypothesized that the collapse of cavitation bubbles produces hypervelocity indentations at very high strain rates causing the metal to splash into the surrounding fluid. During such a splash, a number of well-formed and partially formed spheroids are produced. The cylindrical and needle shaped particles may represent the stem of the splashing metal frozen spontaneously during splash. The surface of the spheres indicate the freezing and oxidation phenomenon. Preliminary calculations of the probable temperature rise on the surface of the material support the general trend of experimental evidence. Lead and aluminum experience much larger temperature increases as compared to a material such as monel. This result is in general agreement with the experimetal observation that more spheroids are observed with aluminum. The influences of the heat of fusion and thermal diffusivity need further study.

## References


1. Scott, D. and Mills, G.H., "Spherical Debris - Its Occurrence, Formation and Significance in Rolling Contact Fatigue," *Wear 24*, 1973, 235-242.
2. Wescott, V.C., "Survey of Wear Processes and the Particles Resulting from Wear by Means of a Ferrograph," TransSonics Incorporated Technical Report to Office of Naval Research, October 1972.
3. Doroff, S.W., Miller, R.S., Thiruvengadam, A.P., Wescott, V.C., "Spheroidal Particles Produced by Cavitation Erosion," *Nature*, Vol. 247, No. 5440, pp. 363-364, February 8, 1974.
4. Loy B. and McCallum, R., "Mode of Formation of Spherical Particles in Rolling Contact Fatigue," *Wear 24*, 1973, 219-228.
5. Rayleigh, Lord, "On the Pressure Developed in a Liquid During the Collapse of a Spherical Cavity," Phil. Mag. 34, Series 4, 1917, 94-98.
6. Plesset, M.S. and Chapman, R.B., "Collapse of an Initially Spherical Vapor Cavity in the Neighborhood of a Solid Boundary," Rep. 85-49, Cal, Inst. of Tech., Div. of Engr., June 1970.

# Research Notes

## Preservatives for the Parthenon

Scientists at the Naval Research Laboratory have applied a variety of fluoropolymer coatings to samples of Acropolis marble from Athens for evaluation as protective barriers against environmental damage to ancient structures, including the 2400-year-old Parthenon temple. The results of the evaluation to be performed in Greece are awaited with great interest, since the problem of preserving monuments and structures of historical value against the ravages of modern air pollution exists worldwide.

These coatings were brought to the attention of Professor Theodore Skoulikidis, Director of the National Technical University in Athens, by Drs. John D. Bultman and Rex A. Neihof last summer during a trip to the Mediterranean aboard the research ship USNS HAYES.

Professor Skoulikidis has been studying the use of coatings for the preservation of marble and concluded that fluoropolymers would be exceptionally promising for this application, but he had been unable to locate a source of suitable materials.

Upon learning of the NRL fluoropolymer coatings, Professor Skoulikidis suggested a joint research effort in which he would supply small samples of Acropolis marble for NRL to coat and return to Greece for evaluation.

Eight coating systems consisting of clear fluoroepoxy and fluoropolyurethane polymers were applied to the marble samples. These fluoropolymers, which had been conceived and synthesized at NRL by Dr. Griffith and Mr. O'Rear, were developed into practical paint systems for Navy applications as non-toxic, fouling-release coatings for the external hulls of ships, easily-cleaned bilge and holding tank coatings, water-resistant encapsulants for electronic equipment, ice release surfaces, and barriers against marine borers for wood.

## Proton-Beam Pumping of Gas Laser

The first intense proton-beam pumping of a gas laser has been demonstrated by a team of scientists at the Naval Research Laboratory. They report preliminary measurements which suggest that proton-beam pumping may be more efficient than its electron beam counterpart because of the large number of ionizations per unit path length for protons in rare gases. Strong stimulated emission in the Argon-Nitrogen laser system at 358 and 381 nanometers (nm), and in Xenon fluoride at 351 and 353 nm has been observed.

The laser gas mixture was irradiated by a 450 kiloelectron Volt pulsed beam of protons from a reflex tetrode powered by a Seven Ohm Line (SOL) generator.

XeF laser pulses exceeding 4 millijoules were obtained for nonoptimized cavity conditions when 0.5 Joules of proton energy were deposited in the laser cell, yielding a laser efficiency of 0.8%. The use of neon along with higher operating pressures and an optimized optical cavity is expected to increase the laser efficiency.

# System for Analyses of Earth's Magnetic Field

Scientists at the Naval Research Laboratory have developed a novel computer which provides real-time acquisition and processing of aeromagnetic data for studies of the dynamic processes which act upon the Earth's crust and upper mantle.

Robert Feden, principal investigator for the program, says his system allows rapid analysis and dissemination of information to the scientific community concerning anomalies in the Earth's magnetic field.

Magnetic anomaly interpretation is widely used in age dating the Earth's crust and permits researchers to correlate data on a global scale. An area north of New Zealand has been studied using the NRL's P3A research aircraft. The tests, designed to determine magnetic lineation, age and tectonic patterns (deformations of the Earth's crust and forces which produce them), covered the southern end of the Havre Trough and the South Fiji Basin.

A magnetic anomaly symmetry during the past 5 million years was detected over the axis of the Havre Trough and NE-SW trending anomalies from 27-28 million years old were found in the South Fiji Basin.

The data provide evidence for two major sea-floor spreading events north of New Zealand: the formation of the Fiji Basin and the later, continuing formation of the Havre Trough-Lau Basin System.

Research is continuing and NRL has recently completed additional studies in the region which will increase knowledge of the processes forming and transforming ocean features.

A more thorough understanding of these processes will enable Navy researchers to predict locations of topographic features.

This project is sponsored by the Office of Naval Research.

---

**NAVAL RESEARCH REVIEWS** publishes highlights of research conducted by Navy laboratories and contractors and describes important naval experimental facilities. Manuscripts submitted for publication, correspondence concerning prospective articles, and changes of address, should be directed to Code 730, Office of Naval Research, Arlington, Va. 22217. Requests for subscriptions should be directed to the Superintendent of Documents, U.S. Government Printing Office, Washington, D.C., 20402. Subscription price: $6.50 per year in the U.S. and Canada; $8.15 per year, foreign; $0.55 per individual copy. The issuance of this periodical approved in accordance with Dept. of the Navy publications and printing regulations.

*Editor:* WILLIAM J. LESCURE

NAVSO P-510

*Associate Editors:*

L. LARMORE, ONR PASADENA
G. SANDOZ, ONR CHICAGO
A.L. POWELL, ONR BOSTON
D.A. PATTERSON, NAVAL RESEARCH LABORATORY

# IN THIS ISSUE

VOL. XXXI, NO. 5



## Cover Caption

*A partially formed spherical particle was found among the erosion debris which contained the break away portion of the stem as shown in the SEM micrograph. This laboratory produced particle is like those found in bearing surfaces and lubricating oils.* *See page 16.*

**DEPARTMENT OF THE NAVY**
**OFFICE OF NAVAL RESEARCH**
**ARLINGTON, VA. 22217**

**OFFICIAL BUSINESS**

*PENALTY FOR PRIVATE USE, $300.*

POSTAGE AND FEES PAID
DEPARTMENT OF THE NAVY
DoD-316
CONTROLLED CIRCULATION RATE

U.S.MAIL